Delamination of a strong film from a ductile substrate during indentation unloading

Abdul-Baqi, A.; van der Giessen, Erik

Published in:
Journal of Materials Research

DOI:
10.1016/S0040-6090(00)01344-4

Publication date:
2001

ELSEVIER

Thin Solid Films 381 (2001) 143–154

thin solid films

www.elsevier.com/locate/tsf

Indentation-induced interface delamination of a strong film on a ductile substrate

A. Abdul-Baqi, E. Van der Giessen*

Delft University of Technology, Koiter Institute Delft, Mekelweg 2, 2628 CD Delft, The Netherlands

Received 15 January 2000; received in revised form 12 July 2000; accepted 12 July 2000

Abstract

The objective of this work is to study indentation-induced delamination of a strong film from a ductile substrate. To this end, spherical indentation of an elastic–perfectly plastic substrate coated by an elastic thin film is simulated, with the interface being modeled by means of a cohesive surface. The constitutive law of the cohesive surface includes a coupled description of normal and tangential failure. Cracking of the coating itself is not included and residual stresses are ignored. Delamination initiation and growth are analyzed for several interfacial strengths and properties of the substrate. It is found that delamination occurs in a tangential mode rather than a normal one and is initiated at two to three times the contact radius. It is also demonstrated that the higher the interfacial strength, the higher the initial speed of propagation of the delamination and the lower the steady state speed. Indentation load vs. depth curves are obtained where, for relatively strong interfaces, the delamination initiation is imprinted on this curve as a kink.

Keywords: Adhesion; Coatings; Hardness; Interfaces

1. Introduction

Indentation is one of the traditional methods to quantify the mechanical properties of materials and during the last decades it has also been advocated as a tool to characterize the properties of thin films or coatings. At the same time, for example for hard wear-resistant coatings, indentation can be viewed as an elementary step of concentrated loading. For these reasons, many experimental as well as theoretical studies have been devoted to indentation of coated systems during recent years.

Proceeding from a review by Page and Hainsworth [1] on the ability of using indentation to determine the properties of thin films, Swain and Menčik [2] have considered the possibility to extract the interfacial energy from indentation tests. Assuming the use of a small spherical indenter, they identified five different classes of interfacial failure, depending on the relative properties of film and substrate (hard/brittle vs. ductile), and the quality of the adhesion. Except for elastic complaint films, they envisioned that plastic deformation plays an important role when indentation is continued until interface failure. As emphasized further by Bagchi and Evans [3], this makes the deduction of the interface energy from global indentation load vs. depth curves a complex matter.

Viable procedures to extract the interfacial energy will depend strongly on the precise mechanisms involved during indentation. In the case of ductile films on a hard substrate, coating delamination is coupled to

* Corresponding author. Tel.: +31-15-278-65002150; fax: +31-15-278-2150.

E-mail address: e.vandergiessen@wbmt.tudelft.nl (E. Van der Giessen).

0040-6090/01/$ - see front matter
PII: S0040-6090(00)01344-4

plastic expansion of the film with the driving force for delamination being delivered via buckling of the film. The key mechanics ingredients of this mechanism have been presented by Marshall and Evans [4], and Kriese and Gerberich [5] have recently extended the analysis to multilayer films. On the other hand, coatings on relatively ductile substrates often fail during indentation by radial and in some cases circumferential cracks through the film. The mechanics of delamination in such systems has been analyzed by Drory and Hutchinson [6] for deep indentation with depths that are two to three orders of magnitude larger than the coating thickness. The determination of interface toughness in systems that show coating cracking has been demonstrated recently by, e.g. Wang et al. [7]. In both types of material systems there have been reports of 'fingerprints' on the load–displacement curves in the form of kinks [5,8,9], in addition to the reduction of hardness (softening) envisaged in [2]. The origin of these kinks remains somewhat unclear, however.

A final class considered in [2] is that of hard, strong coatings on ductile substrates, where Swain and Menčik hypothesized that indentation with a spherical indenter would not lead to cracking of the coating but just to delamination. This class has not yet received much attention, probably because most deposited coatings, except diamond or diamond-like carbon, are not sufficiently strong to remain intact until delamination. On the other hand, it provides a relatively simple system that serves well to gain a deep understanding of the coupling between interfacial delamination and plasticity in the substrate. An analysis of this class is the subject of this paper.

In the present study, we perform a numerical simulation of the process of indentation of thin elastic film on a relatively softer substrate with a small spherical indenter. The indenter is assumed to be rigid, the film is elastic and strong, and the substrate is elastic–perfectly plastic. The interface is modeled by a cohesive surface, which allows to study initiation and propagation of delamination during the indentation process. Separate criteria for delamination growth are not needed in this way. The aim of this study is to investigate the possibility and the phenomenology of interfacial delamination. Once we have established the critical conditions for delamination to occur, we can address more design-like questions, such as what is the interface strength needed to avoid delamination. We will also study the 'fingerprint' left on the load–displacement curve by delamination, and see if delamination itself can lead to kinks as mentioned above in other systems. It is emphasized that the calculations assume that other failure events, mainly through-thickness coating cracks, do not occur.

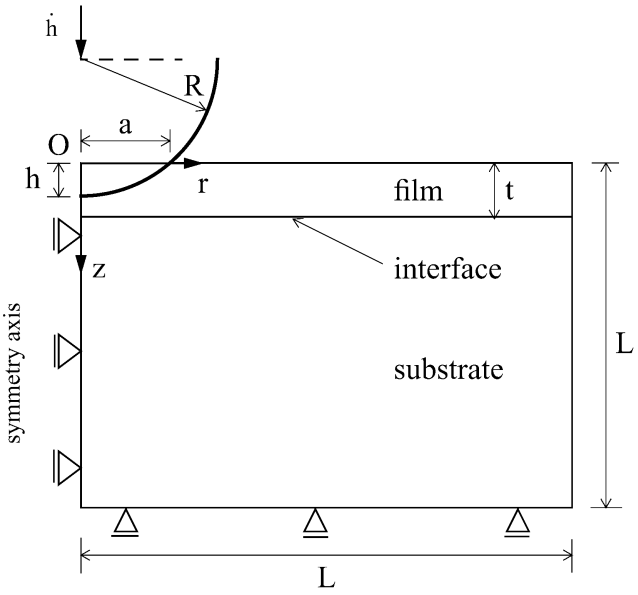

Fig. 1. Illustration of the boundary value problem analyzed in this study.

2. Problem formulation

2.1. Governing equations

We consider a system comprising an elastic–perfectly plastic material (substrate) coated by an elastic thin film and indented by a spherical indenter. The indenter is assumed rigid and only characterized by its radius R. Assuming both coating and substrate to be isotropic, the problem is axisymmetric, with radial coordinate r and axial coordinate z in the indentation direction, as illustrated in Fig. 1. The film is characterized by its thickness t and is bonded to the substrate by an interface, which will be specified in the next section. The substrate is taken to have a height of $L-t$ and radius L, with L large enough so that the solution is independent of L and the substrate can be regarded as a half space.

The analysis is carried out numerically using a finite strain, finite element method. It uses a Total Lagrangian formulation in which equilibrium is expressed in terms of the principle of virtual work as

$$\int_v \tau^{ij}\delta\eta_{ij}\mathrm{d}v + \int_{S_i} T_\alpha \delta\Delta_\alpha \mathrm{d}S = \int_{\partial v} t^i \delta u_i \mathrm{d}s. \qquad (1)$$

Here, v is the total $L\times L$ region analyzed and ∂v is its boundary, both in the undeformed configuration. With $x^i=(r,\ z,\ \theta)$ the coordinates in the undeformed configuration, u_i and t^i are the components of displacement and traction vector, respectively; τ^{ij} are the

components of Second Piola–Kirchhoff stress while η_{ij} are the dual Lagrangian strain components. The latter are expressed in terms of the displacement fields in the standard manner,

$$\eta_{ij} = 1/2\left(u_{i,j} + u_{j,i} + u^k_{,i} u_{k,j}\right) \tag{2}$$

where a comma denotes (covariant) differentiation with respect to x^i. The second term in the left-hand side is the contribution of the interface, which is here measured in the deformed configuration ($S_i = \{z = t\}$). The (true) traction transmitted across the interface has components T_α, while the displacement jump is Δ_α, with α being either the local normal direction ($\alpha = n$) or the tangential direction ($\alpha = t$) in the (r, z) plane. Here, and in the remainder, the axisymmetry of the problem is exploited, so that $u_3 = t^3 = \tau^{i3} = \eta_{i3} = 0$.

The precise boundary conditions are illustrated in Fig. 1. The indentation process is performed incrementally with a constant indentation rate $\dot{h}$. Outside the contact area with radius a in the reference configuration, the film surface is stress free,

$$t^r(r,0) = t^z(r,0) = 0 \quad \text{for } a \le r \le L. \tag{3}$$

Inside the contact area we assume perfect sticking conditions so that the displacement rates are controlled by the motion of the indenter, i.e.

$$\dot{u}_z(r,0) = \dot{h}, \quad \dot{u}_r(r,0) = 0 \quad \text{for } 0 \le r \le a. \tag{4}$$

Numerical experiments using perfect sliding conditions instead have shown that the precise boundary conditions only have a significant effect very close to the contact area and do not alter the results for delamination to be presented later. The indentation force F is computed from the tractions in the contact region,

$$F = \int_0^a t^z(r,0) 2\pi r \, \mathrm{d}r. \tag{5}$$

The substrate is simply supported at the bottom, so that the remaining boundary conditions read

$$\begin{aligned} u_z(r,L) &= 0 \quad \text{for } 0 \le r \le L; \\ u_r(0,z) &= 0 \quad \text{for } 0 \le z \le L. \end{aligned} \tag{6}$$

However the size L will be chosen large enough that the solution is independent from the precise remote conditions.

The Eqs. (1) and (2) need to be supplemented with the constitutive equations for the coating and the substrate, as well as the interface. As the latter are central to the results of this study, these will be explained in detail in the forthcoming section. The substrate is supposed to be a standard isotropic elastoplastic material with plastic flow being controlled by the von Mises stress. For numerical convenience, however, we adopt a rate-sensitive version of this model, expressed by

$$\dot{\eta}^p_{ij} = 3/2 \frac{s_{ij}}{\sigma_e} \dot{\varepsilon}^p, \quad \dot{\varepsilon}^p = \dot{\varepsilon}_y \left(\frac{\sigma_e}{\sigma_y}\right)^n \tag{7}$$

for the plastic part of the strain rate, $\dot{\eta}^p_{ij} = \dot{\eta}_{ij} - \dot{\eta}^e_{ij}$. Here $\sigma_e = \sqrt{3/2 s_{ij} s^{ij}}$ is the von Mises stress, expressed in terms of the deviatoric stress components s_{ij}, n is the rate sensitivity exponent and $\dot{\varepsilon}_y$ is a reference strain rate. In the limit of $n \to \infty$, this constitutive model reduces to the rate-independent von Mises plasticity with yield stress σ_y. Values of n on the order of 100 are frequently used for metals (see e.g. [10]), so that the value of σ_e, at yield is within a few percent of σ_y. The elastic part of the strain rate, $\dot{\eta}^e_{ij}$, is given in terms of the Jaumann stress rate as

$$\overset{\nabla}{\tau}{}^{ij} = R^{ijkl} \dot{\eta}^e_{kl} \tag{8}$$

with the elastic modulus tensor R^{ijkl} being determined by the Young modulus E_s and Poisson's ration ν_s, (subscript s for substrate).

The coating is assumed to be a strong, perfectly elastic material with Young's modulus E_f and Poisson's ration ν_f (subscript f for film).

The above equations, supplemented with the constitutive law for the interface to be discussed presently, form a non-linear problem that is solved in a linear incremental manner. For this purpose, the incremental virtual work statement is furnished with an equilibrium correction to avoid drifting from the true equilibrium path. Time integration is performed using the forward gradient version of the viscoplastic law (7) due to Peirce et al. [11].

2.2. The cohesive surface model

In the description of the interface as a cohesive surface, a small displacement jump Δ between the film and substrate is allowed, with normal and tangential components Δ_n, and Δ_t, respectively. The interfacial behaviour is specified in terms of a constitutive equation for the corresponding traction components T_n and T_t at the same location. The constitutive law we adopt in this study is an elastic one, so that any energy dissipation associated with separation is ignored. Thus, it can be specified through a potential, i.e.

$$T_\alpha = -\frac{\partial \phi}{\partial \Delta_\alpha} \quad (\alpha = n,t). \tag{9}$$

The potential reflects the physics of the adhesion between the coating and substrate. Here, we use the

potential ϕ that was given by Xu and Needleman [12], i.e.

$$\phi = \phi_n + \phi_n \exp\left(-\frac{\Delta_n}{\delta_n}\right)\left\{\left[1 - r + \frac{\Delta_n}{\delta_n}\right]\frac{1-q}{r-1} - \left[q + \left(\frac{r-q}{r-1}\right)\frac{\Delta_n}{\delta_n}\right]\exp\left(-\frac{\Delta_t^2}{\delta_t^2}\right)\right\} \quad (10)$$

with ϕ_n and ϕ_t the normal and tangential works of separation ($q = \phi_t/\phi_n$), δ_n and δ_t two characteristic lengths, and r a parameter that governs the coupling between normal and tangential separation. The corresponding traction–separation laws from Eq. (9) read

$$T_n = \frac{\phi_n}{\delta_n}\exp\left(-\frac{\Delta_n}{\delta_n}\right)\left\{\frac{\Delta_n}{\delta_n}\exp\left(-\frac{\Delta_t^2}{\delta_t^2}\right) + \frac{1-q}{r-1}\left[1 - \exp\left(-\frac{\Delta_t^2}{\delta_t^2}\right)\right]\left[r - \frac{\Delta_n}{\delta_n}\right]\right\}; \quad (11)$$

$$T_t = 2\frac{\phi_n}{\delta_n}\left(\frac{\delta_n}{\delta_t}\right)\frac{\Delta_t}{\delta_t}\left\{q + \left(\frac{r-q}{r-1}\right)\frac{\Delta_n}{\delta_n}\right\}\exp\left(-\frac{\Delta_n}{\delta_n}\right)\exp\times\left(-\frac{\Delta_t^2}{\delta_t^2}\right). \quad (12)$$

The form of the normal response, $T_n = T_n(\Delta_t = 0)$ is motivated by the universal binding law of Rose et al. [13]. In the presence of tangential separation, $\Delta_t \neq 0$, Eq. (11) is a phenomenological extension of this law, while the tangential response Eq. (12) should be considered as entirely phenomenological. The uncoupled responses, i.e. with $\Delta_t = 0$ ($\Delta_n = 0$) for the normal (tangential) response, are shown in Fig. 2. Both are highly non-linear with a distinction maximum of the normal (tangential) traction of σ_{max} (τ_{max}) which occurs at a separation of $\Delta_n = \delta_n$ ($\Delta_t = \delta_t/\sqrt{2}$). The normal (tangential) work of separation, ϕ_n (ϕ_t), can now be expressed in terms of the corresponding strengths σ_{max} (τ_{max}) as

$$\phi_n = \exp(1)\sigma_{max}\delta_n, \quad \phi_t = \sqrt{1/2\exp(1)}\,\tau_{max}\delta_t. \quad (13)$$

Using Eq. (13) together with the relation $q = \phi_t/\phi_n$, we can relate the uncoupled normal and shear strengths through

$$\sigma_{max} = \frac{1}{q\sqrt{2\exp(1)}}\frac{\delta_t}{\delta_n}\tau_{max} \quad (14)$$

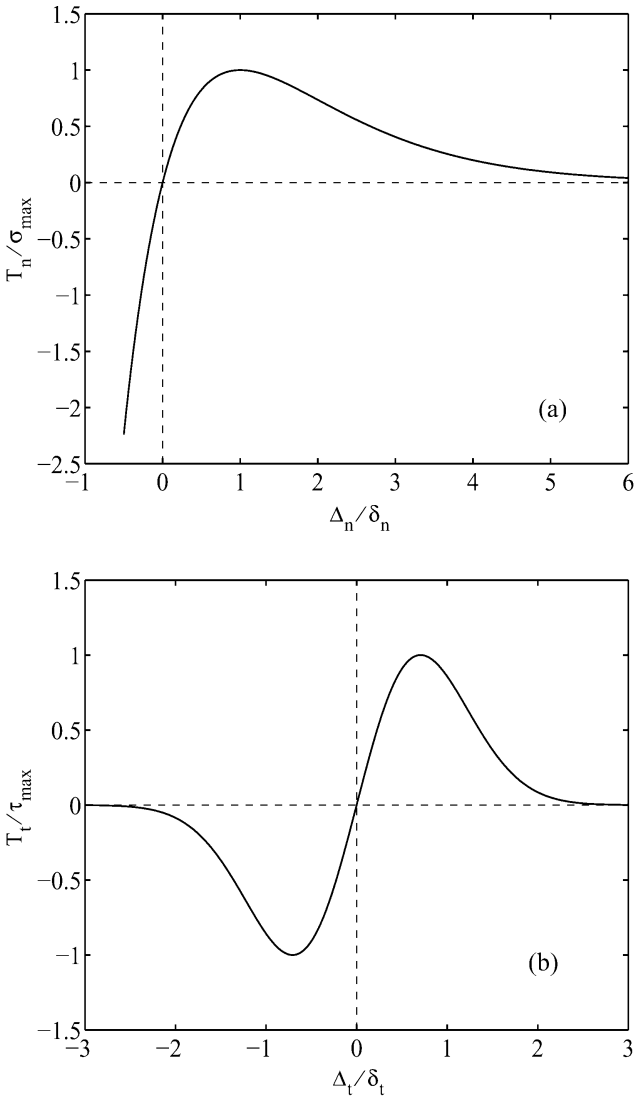

Fig. 2. The uncoupled normal and tangential responses according to the cohesive surface law Eqs. (11) and (12). (a) Normal response $T_n(\Delta_n)$ with $\Delta_t = 0$. (b) Tangential response $T_t(\Delta_t)$ with $\Delta_n = 0$. Both are normalized by their respective peak values, σ_{max} and τ_{max}.

The coupling parameter r can be interpreted as the value of the normal separation Δ_n/δ_n after complete shear separation ($\Delta_t/\delta_t \to \infty$) with $T_n = 0$. Some insight into the coupling between normal and shear response can be obtained from Fig. 3, which shows the maximum shear traction as a function of the normal displacement, i.e. $T_t^{max}(\Delta_n) \equiv T_t(\Delta_t/\delta_t = 1/\sqrt{2}, \Delta_n)$. It is seen that this is quite sensitive to the values of r and q. The maximum shear traction that can be transmitted decreases when there is opening in the normal direction ($\Delta_n > 0$) for all parameter combinations shown. However, in normal compression ($\Delta_n < 0$), the maximum shear stress can either increase or decrease with $-\Delta_n$. An increase appears to be the most realistic, and the parameter values used in the present study ensure this.

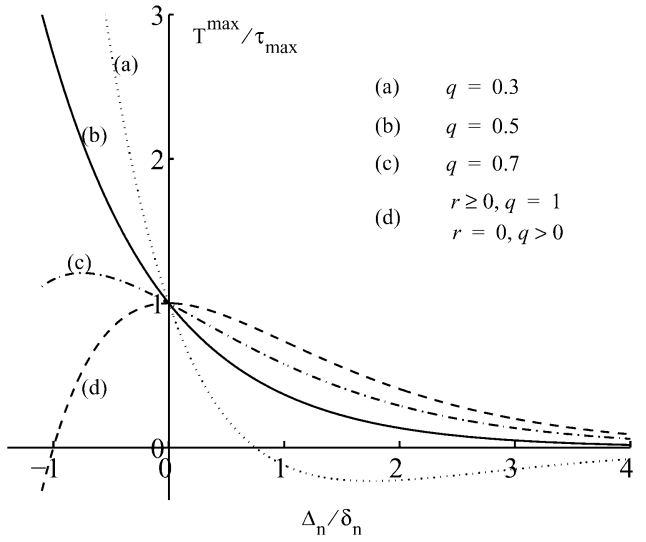

Fig. 3. The maximum shear traction T_t^{max}, normalized by τ_{max} (see Fig. 2), as a function of the normal separation for different combinations of the coefficients r and q. In (a)–(c), $r = 0.5$

3. Results and discussion

3.1. Analysis and parameters

The solution to the problem depends on a number of non-dimensional parameters. We have chosen the following non-dimensional groups:

$$\text{geometry:} \quad \frac{R}{t} \tag{15}$$

$$\text{material:} \quad \frac{E_f}{E_s},\ \frac{\sigma_y}{E_s},\ \nu_f,\ \nu_c \tag{16}$$

$$\text{interface:} \quad q,\ \frac{\delta_n}{t},\ \frac{\delta_n}{\delta_t},\ \frac{\tau_{max}}{\sigma_y},\ r \tag{17}$$

$$\text{loading:} \quad \frac{h}{t},\ \frac{F}{R^2\sigma_y}\left(\frac{t\dot{\varepsilon}_y E_s}{\sigma_y \dot{h}}\right)^{1/(n-1)} \tag{18}$$

Note that the rather complex form of the last loading parameter is dictated by the fact that rate-dependent plasticity, Eq. (7), is governed by the parameters $\dot{\varepsilon}_y$ and σ_y only through the combination $\dot{\varepsilon}_y/\sigma_y^n$. This non-dimensional parameter immediately shows that the indentation force depends on the indentation rate in a rate-dependent material. However, in the limit that $n \to \infty$, the bracketed factor becomes 1, so that the parameter reduces to $F/(R^2\sigma_y)$.

In the results to be presented we focus mainly on the effect of the normalized substrate yield strength σ_y/E_s, which is simply the yield strain, and the normalized interfacial shear strength τ_{max}/σ_y on the initiation and advance of interfacial delamination. The relation between normal and tangential interfacial strengths is given by Eq. (14). Three values of σ_y/E_s, were chosen, namely 0.0025, 0.005 and 0.01. For each value of σ_y/E_s, several values of τ_{max}/σ_y are chosen.

Even though the solution is formally governed by the above-mentioned non-dimensional groups, we have chosen to work primarily in terms of real dimensional values in order to simplify the interpretation. We have used an indenter of radius $R = 0.05$ mm and a film thickness $t = 0.005$ mm. The elastic properties are $E_f = 500$ GPa, $\nu_f = 0.33$, $E_s = 200$ GPa and $\nu_s = 0.33$. The yield stress of the substrate is varied, as discussed above, and the reference strain rate is taken to be $\dot{\varepsilon}_y = 0.1\ \text{s}^{-1}$ with $n = 100$. The indentation is performed under a constant rate $\dot{h} = 1$ mm/s. For a typical value of σ_y/E_s of 0.005, the value of the factor $(t\dot{\varepsilon}_y E_s/\sigma_y \dot{h})^{1/(n-1)}$ in Eq. (18) is 0.977; this is less than 2.5% smaller than the rate-independent limit. For the cohesive surface we have chosen the same values for δ_n, and δ_t, namely 10^{-4} mm. Most of the results to be presented are for $r = 0.5$ and $q = 0.5$, but we will also briefly investigate the sensitivity of the results to these values. As mentioned above, various values of τ_{max} will be considered; it should be noted that by using a constant ratio q, the normal strength σ_{max} varies with τ_{max} according to Eq. (14). The values of τ_{max} to be investigated vary between 0.3 and 1.4 GPa. This corresponds to interfacial energies for shear failure ranging from 35 to 160 J/m^2 which are realistic values for the interface toughnesses for well-adhering deposited films [3].

The size L of the system analyzed (Fig. 1) is taken to be $10R$. This proved to be large enough that the results are independent of L and therefore identical to those for a coated half-infinite medium. The mesh is an arrangement of 19 600 quadrilateral elements, and 21 291 nodes. The elements are built up of four linear strain triangles in a cross arrangement to minimize numerical problems due to plastic incompressibility. To account properly for the high stress gradients under the indenter and for an accurate detection of the contact nodes, the mesh is made very fine locally near the contact area with an element size of $t/10$.

Consistent with the type of elements in the coating and the substrate, linear two-noded elements are used along the interface. Integration of the cohesive surface contribution in Eq. (1) is carried out using two-point Gauss integration. Failure, or delamination, of the interface at any location develops when Δ_α exceeds δ_α. The critical instant is here taken to be when $\Delta_\alpha = \delta_\alpha$. Larger critical values may be used as well [14], but using two or three times δ_α does not significantly change the critical indentation depth or force.

The maximum indentation depth applied in all calcu-

lations is $h_{max} = 2t$. Further indentation can be done, but was not considered relevant since real coatings will have cracked by then and the present model is no longer applicable.

3.2. Perfect interface

For the purpose of reference, we first consider a coated system with a perfect interface, which would correspond to taking $\tau_{max}/\sigma_y \to \infty$. We have analyzed this simply by rigidly connecting the coating to the substrate (cf. also [15,16]). Of particular relevance here, is the stress distribution that develops at the coating–substrate interface. Fig. 4 shows the normal (σ_n) and shear (σ_t) stress components at different indentation depths for the case of $\sigma_y/E_s = 0.0025$. Other values of σ_y/E_s would give the same qualitative behaviour. Note that the radial position r is normalized, for each h, by the current contact radius a.

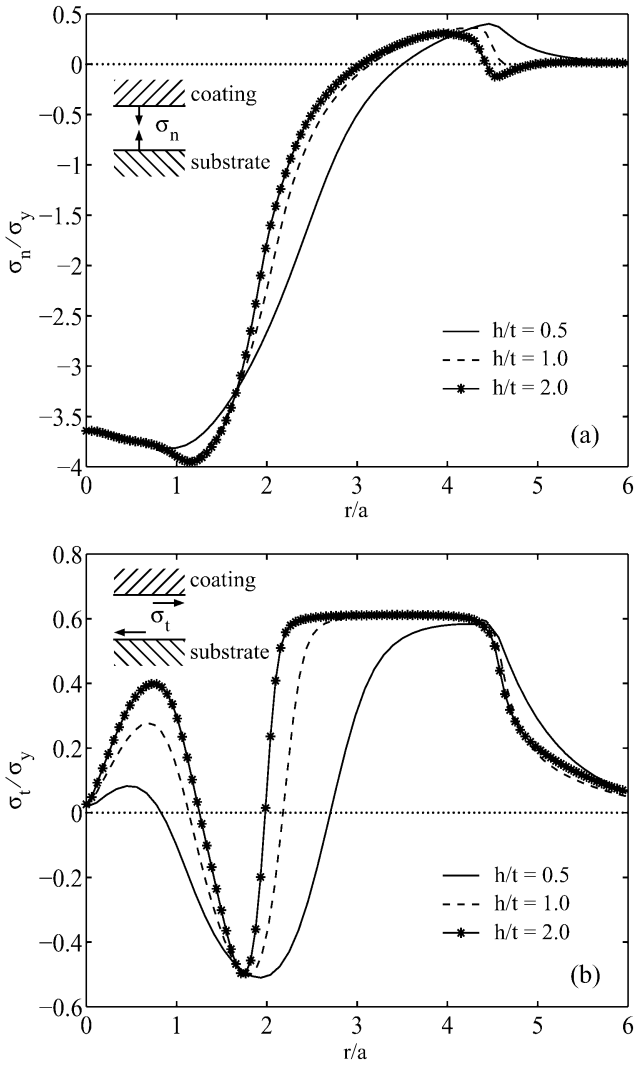

Fig. 4. Interfacial tractions along a perfectly bonded interface at three indentation depths (a is the instantaneous contact radius) for $\sigma_y/E_s = 0.0025$. (a) Normal stress. (b) Shear stress.

In the contact area below the indenter ($r \le a$) the interface is of course under high compression (Fig. 4a). The reason for this stress being the same for all indentation depths shown is that the contact region is contained within the plastic zone in the substrate, which exhibits no hardening. For $r > 3a$ roughly, there is an annular region with an opening normal stress. According to Fig. 4b there are three regions in which the interfacial shear stress exhibits a local maximum (in absolute value): near the edge of the contact radius, at approximately $2a$ and in a region between $3a$ and $5a$. The highest shear stress, roughly $0.6\sigma_y$, is attained in this outer region. Closer examination of the results reveals that this shear stress is caused by the outward radial plastic flow of the substrate under the indenter relative to the coating. The latter is being pulled inwards due to the indentation. This relative motion is opposite to that observed in the calculations of Narasimhan and Biswas [17] who considered a plastically deforming film on a rigid substrate.

The most noteworthy part of the stress distributions in Fig. 4 is that there is an annular region around $r > 3a$ where the shear stresses are larger and the normal stress is positive. This is relevant for delamination because of the coupling between normal and tangential response of the interface. Rephrased in terms of the cohesive surface model used here, the opening normal stress, corresponding to $\Delta_n > 0$, significantly reduces the maximal shear stress before shear failure, as shown in Fig. 3, so that this region $r > 3a$ is a potential location for delamination.

3.3. Initiation of delamination

In the presence of cohesive surface along the interface, a distribution of normal and tangential separations develops, $\Delta_\alpha(r)$, with progressive indentation h. The actual initiation of delamination is identified when $\Delta_n(r) = \delta_n$ or $\Delta_t(r) = \delta_t$ for any r. The indentation depth at this instant is denoted by h_c, the corresponding contact radius is a_c and the critical position is r_c. For all parameter combinations investigated (cf. Section 3.1) we indeed find that delamination occurs by tangential failure, $\Delta_t(r) \ge \delta_t$.

A parameter study has been carried out to determine the dependence of h_c, r_c and a_c on the two key material characteristics: the substrate yield strength σ_y and the interfacial shear strength τ_{max}. This is done by scanning, for three values of σ_y/E_s, several values of the ratio τ_{max}/σ_y. In the case of $\sigma_y/E_s = 0.0025$, the values of τ_{max}/σ_y are 0.6, 0.7, 0.75, 0.8, 0.85 and 0.86, in the case of $\sigma_y/E_s = 0.005$ the values are 0.3, 0.4, 0.5, 0.6, 0.7, 0.75 and 0.8, and in the case of $\sigma_y/E_s = 0.01$

the values are 0.2, 0.3, 0.4, 0.5, 0.6 and 0.7. For each σ_y/E_s, higher values of τ_{max}/σ_y were considered but above a certain value delamination was not found. The fact that there is a limiting value for the interfacial strength above which delamination is prevented will be discussed in the next subsection.

Fig. 5 summarizes the obtained values of h_c, r_c, and a_c, for the various cases. Fig. 5a shows that for each of the three substrate yield strengths, r_c increases with the interface strength τ_{max}/σ_y in proportion with the indentation depth h_c. It should be noted that the direct proportionality between r_c and h_c is valid for the range of interface stresses considered here, but breaks down at much smaller strengths. The strengths considered here are such that the indentation depth has to reach roughly the coating thickness t before delamination occurs. The radius at which delamination then initiates is seen to be on the order of the indenter radius R which here is $10t$. Fig. 5b shows that this delamination radius is between two and four times the contact radius a, this factor depending on both interface strength and substrate yield strength. For $\sigma_y/E_s = 0.0025$, we find $r_c/R > 3a_c/R$, which is consistent with the expectation in the previous section.

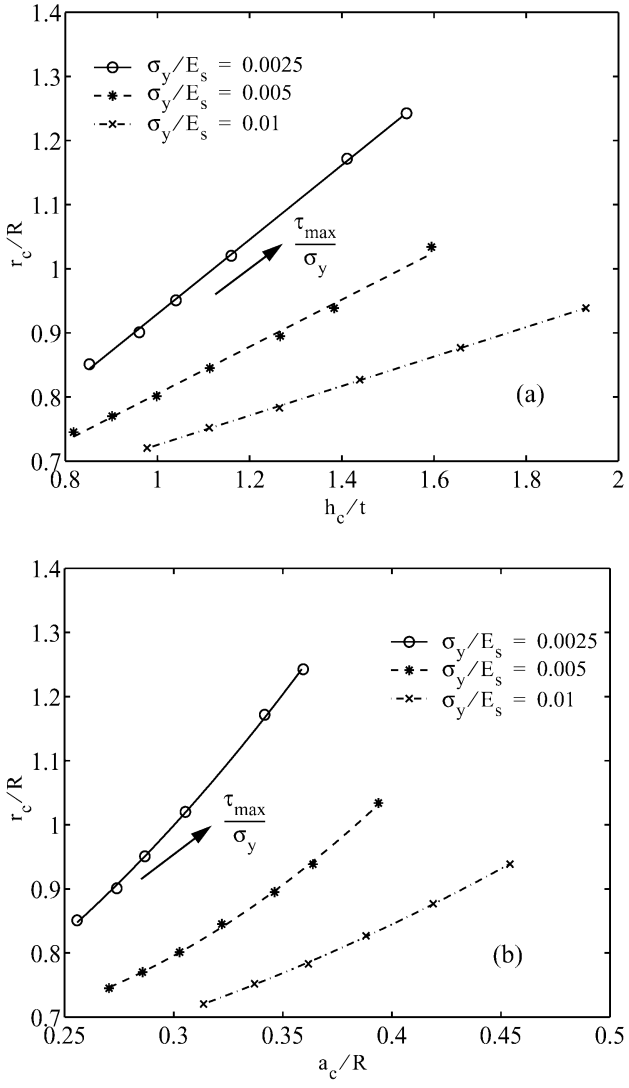

Fig. 5. (a) Location of delamination initiation r_c vs. critical indentation depth h_c. (b) r_c vs. contact radius at delamination initiation. Discrete points are results from the numerical computations; the lines are (a) linear (see Eq. (19)) and (b) second degree polynomial fits. The arrows indicate the direction of increasing τ_{max}/σ_y.

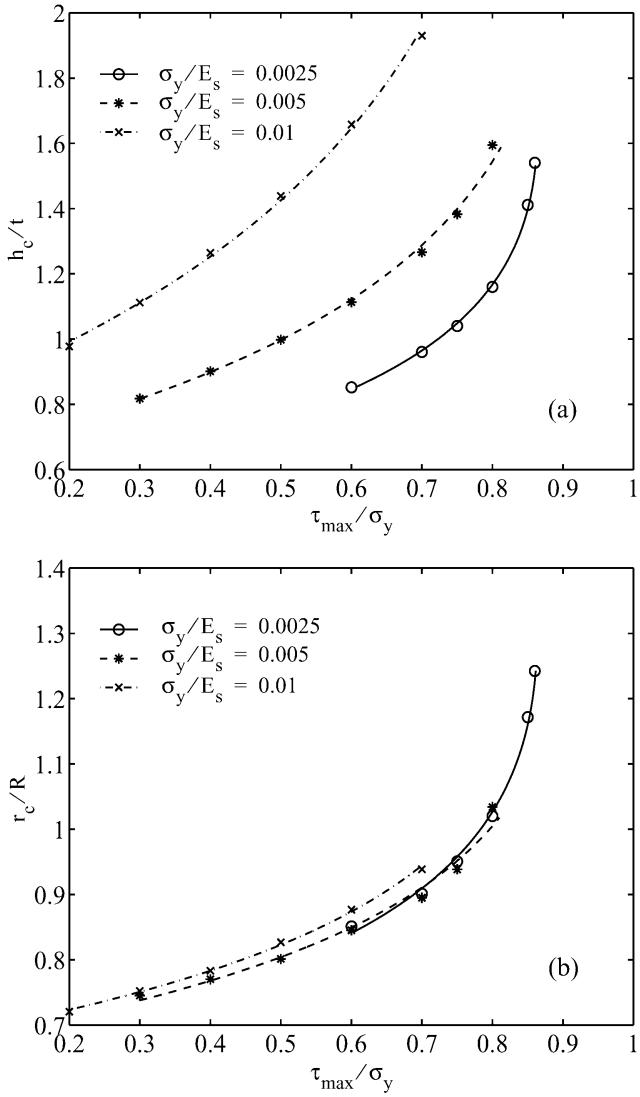

Fig. 6. (a) Critical indentation depth h_c/t and (b) critical delamination radius r_c/R vs. relative interfacial strength τ_{max}/σ_y. Discrete points are results from the numerical computations; the lines are according to fits: (a) Eq. (21); (b) Eq. (22).

The same data are re-plotted in Fig. 6 but now as a function of the ratio between interface and substrate yield strength. We see that both h_c and r_c increase non-linearly with τ_{max}/σ_y. Contrary to r_c, which appears to be depending practically only on τ_{max}/σ_y (Fig. 6b), the indentation depth h_c, is quite a strong function of the substrate yield strain (Fig. 6a). The latter strongly indicates that plastic deformation in the substrate is a

key factor in determining whether or not delamination takes place (we will return to this later).

The results presented in Fig. 5 can be fitted quite accurately by the following relationships:

$$r_c/R = a_1(h_c/t) + a_2, \tag{19}$$

$$(\tau_{max}/\sigma_y)(r_c/R)^2 = a_3(h_c/t) + a_4, \tag{20}$$

The least squares method has been used to obtain the coefficients a_1, through a_4 for the best fit for each of the three values of σ_y/E_s (see Table 1). The relationships (19) and (20) can be combined to give

$$(\tau_{max}/\sigma_y)(a_1(h_c/t) + a_2)^2 = a_3(h_c/t) + a_4, \tag{21}$$

$$a_1(\tau_{max}/\sigma_y)(r_c/R)^2 = a_3(r_c/R - a_2) + a_1a_4, \tag{22}$$

which have then been plotted in Fig. 6. It is seen that they give a reasonable representation to the numerical results over the range of parameters considered here. As mentioned before, the critical indentation depth differs from the trend in Fig. 5 for much smaller values of the interface strength so that extreme care must be taken by extrapolation of Eqs. (19)–(22) outside the considered parameter range.

3.4. Strength limit to delamination

As mentioned before, there is value of τ_{max}/σ_y beyond which delamination does not take place. This value is seen in Fig. 6 to be dependent on σ_y/E_s and, upon closer examination, is related to the coupling between normal and tangential behaviour of the interface. In the absence of this coupling, the shear stress along the interface is limited by the plastic flow in the substrate. In the time-independent limit, $n \to \infty$ in Eq. (7), we have $\sigma_e \le \sigma_y$ so that the maximum value that the shear stress can reach at the interface is $\sigma_y/\sqrt{3}$; when plasticity is slightly rate-dependent as here ($n = 100$) this value can be somewhat larger but $\sigma_y/\sqrt{3}$ is still a very good estimate. Hence, if the interface response is not coupled, delamination is not possible for strengths τ_{max} exceeding $\sigma_y/\sqrt{3}$. The reason for which we find delamination in Fig. 6 at higher τ_{max}/σ_y must be attributed to the coupling in the interface behaviour as described by Eqs. (11) and (12).

Table 1
Coefficients for fitting relations Eqs. (19)–(22)

σ_y/E_s	a_1	a_2	a_3	a_4
0.0025	1.3072	−0.6828	0.5799	0.3497
0.005	0.8863	−0.5610	0.3672	0.4377
0.01	0.5403	−0.4316	0.2298	0.4954

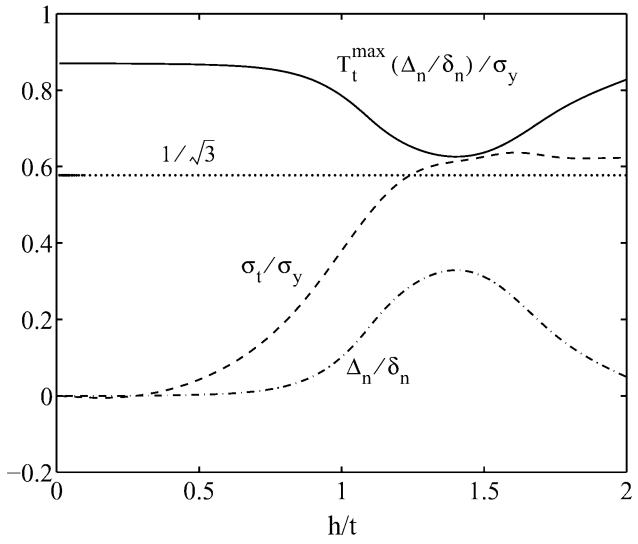

Fig. 7. Evolution with indentation depth h of shear stress σ_t, normal opening Δ_n and corresponding peak tangential traction $T_t^{max}(\Delta_n)$ at $r = 1.24R$.

In the presence of coupling, the maximal tangential traction T_t^{max} at any point along the interface depends on the local normal displacement Δ_n, as shown in Fig. 3. The interfacial region that is of interest then is $r > 3a$ or so, where a tensile interface stress develops during indentation (Fig. 4a), since the corresponding normal opening of the cohesive surface reduces the local shear strength T_t^{max}. Fig. 7 demonstrates this coupling for the case $\sigma_y/E_s = 0.0025$ and $\tau_{max}/\sigma_y = 0.87$, for which delamination did not occur. This figure shows the evolution of Δ_n, σ_t and $T_t^{max}(\Delta_n)$ with indentation depth at $r = 1.24R$ (this is the location where delamination does initiate when $\tau_{max}/\sigma_y = 0.86$). We see that the local shear stress at the interface gradually increases to a value of approximately $\sigma_y/\sqrt{3}$, which evidences that the plastic zone gradually engulfs this point. As this occurs, Δ_n, increases until a certain indentation depth and the effective shear strength T_t^{max} decreases. However, just before T_t^{max} would coincide with σ_t and delamination would initiate, the normal opening starts to decrease and delamination becomes excluded.

Fig. 8 summarizes the limiting values of the interfacial shear strength τ_{max} for the various cases analyzed and plots them directly vs. the substrate yield strength. There appears to be a rather good linear correlation over the range considered, with the deviation from the line $\sigma_y/\sqrt{3}$ increasing with σ_y. The figure also shows the two values for interfaces characterized by different values of $q = \phi_t/\phi_n$ than 0.5, namely $q = 0.3$ and 0.7. According to Fig. 3, a smaller value of q, for example,

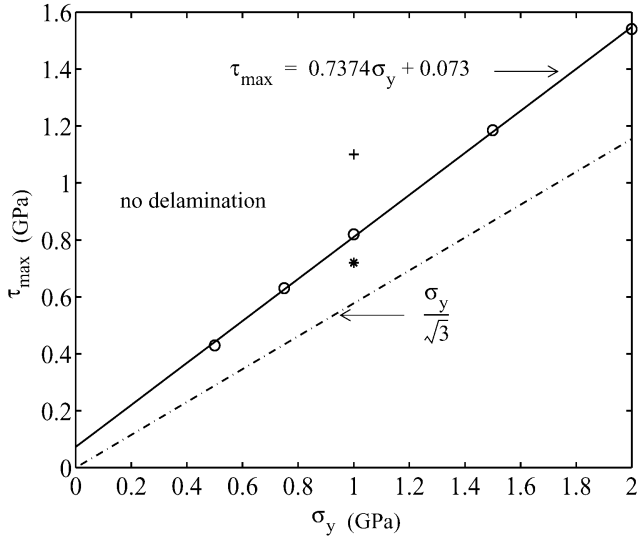

Fig. 8. The interfacial shear strength τ_{max} above which delamination is excluded as a function of the substrate yield stress σ_y. Open circles are the numerical results, while the solid line is a linear fit (the dash-dotted line is the limit in the absence of coupling between normal and tangential separation in the interface). The symbols + and * represent isolated results for $q = 0.3$ and $q = 0.7$, respectively.

implies a stronger reduction of the interfacial shear strength. Hence, the smaller q, the larger the value of τ_{max} that suppresses shear delamination. It is seen from Fig. 8 that the result is quite sensitive to the precise value of q.

3.5. Propagation of delamination

After delamination initiates at the location r_c and at a corresponding indentation depth h_c, it propagates as a shear crack in both directions: towards and away from the indenter. The tip of the zone that propagates towards the indenter gets arrested after a short time because of the compressive normal traction close to the contact area as seen in Fig. 4a. The leading tip of the delaminated zone keeps propagating with continued indentation. Fig. 9a shows the leading tip location, r_f/R, as a function of the indentation depth, h/t, for the case of $\sigma_y/E_s = 0.0025$ (other values of σ_y/E_s show the same qualitative behaviour), and for four different values of interfacial strength. The width of the ring-shaped delaminated area, $(r_f - r_i)/R$, is shown in Fig. 9b as a function of the indentation depth. Since the indentation rate $\dot{h}$ is constant, the propagation speed $\dot{r}_f$ can be expressed as given by

$$\dot{r}_f = \dot{h}\frac{R}{t}\frac{\partial(r_f/R)}{\partial(h/t)}$$

so that it is simply $\dot{h}(R/t)$ times the slope of the curves in Fig. 9a. In each of the four cases shown, delamination starts off with a relatively high speed and reaches a constant steady-state speed after traveling a certain distance from the initiation point. The reason for this is that the dominant driving force for initial propagation is the elastic energy stored in the system; once this energy gets released, it gives rise to more or less instantaneous growth which is just limited here by the rate at which plastic deformation can evolve in the substrate. On the other hand, the steady state propagation is predominantly driven by the indentation process which is performed at a constant rate, thus explaining the constant steady-state propagation speed.

It is of interest to mention here that for some parameter combinations, such as $\sigma_y/E_s = 0.01$ and $\tau_{max}/\sigma_y = 0.7$, we encounter numerical instabilities after the onset of delamination. We attribute this to the stored elastic energy in these cases being so large that ellipticity of the problem is locally lost when this energy

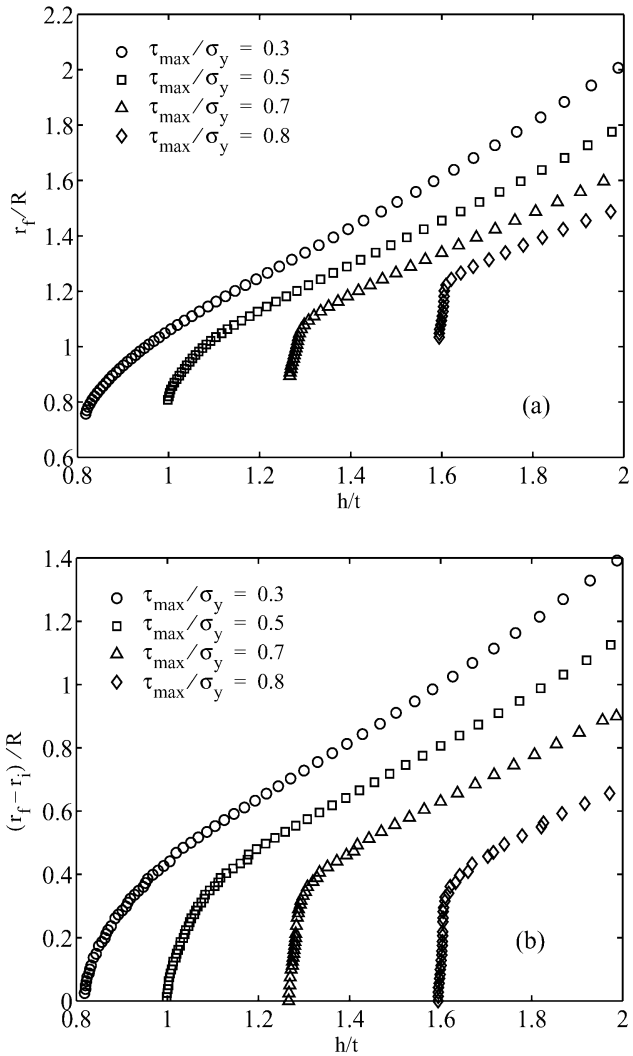

Fig. 9. (a) Location of the leading tip of the delaminated zone, r_f, vs. indentation depth h. (b) The width of the ring-shaped delaminated zone, $r_f - r_i$, vs. indentation depth h. This figure is for the case of $\sigma_y/E_s = 0.0025$, and several values of interfacial strengths.

is released. More advanced solution procedures are necessary to handle this.

To further demonstrate the interaction between delamination and plasticity in the substrate, Fig. 10 shows the distribution of the Von Mises effective stress σ_e in the indented region for $h/t = 1.5$. The particular case shown is for $\tau_{max}/\sigma_y = 0.8$ and $\sigma_y/E_s = 0.0025$. For the purpose of comparison, the distribution for the case of a perfectly bonded interface is included as well [Fig. 10a]. The region in the substrate where the value of σ_e is close to σ_y signifies the region of substantial plastic deformation (note that we are using viscoplasticity so that σ_e is not limited to σ_y). The delaminated zone in Fig. 10b is identified by a white line, and extends from $r_i \approx 0.04$ mm to $r_f \approx 0.07$ mm. It initiated at an indentation depth of $h_c/t = 1.16$ and a critical radius of $r_c \approx 0.05$ mm. Comparison of the two plots shows, first of all, that a plastic region has developed near the leading tip of this zone with a size on the order of the coating thickness. This plastic zone moves with the propagating tip of the delamination zone. Apparently, there is a stress concentration around the tip of the delaminated zone which induces local plastic flow in the substrate. The second difference between Fig. 10a and b is that a perfectly bonded interface induces a plastic zone in the substrate that is somewhat larger than in the case of a finite-strength interface. This is attributed to the fact that interfacial delamination serves as another mechanism for stress relaxation in the system. Except for the near-tip region of the delaminated zone, this tends to reduce the necessity for stress relaxation by plastic deformation, thereby reducing the overall dimension of the plastic zone.

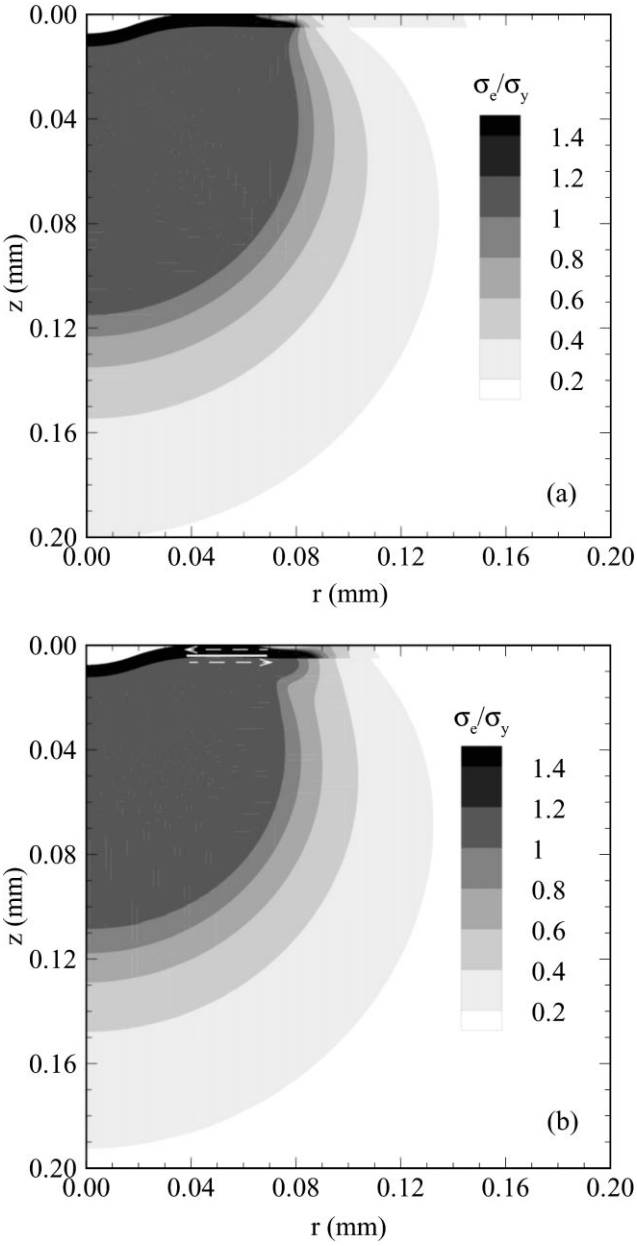

Fig. 10. Contours of the Von Mises effective stress at $h/t = 1.5$ for $\sigma_y/E_s = 0.0025$. (a) Perfectly bonded interface; (b) finite-strength interface with $\tau_{max}/\sigma_y = 0.8$. The white line in (b) denotes the delaminated zone, the arrows indicating the direction of interfacial shear.

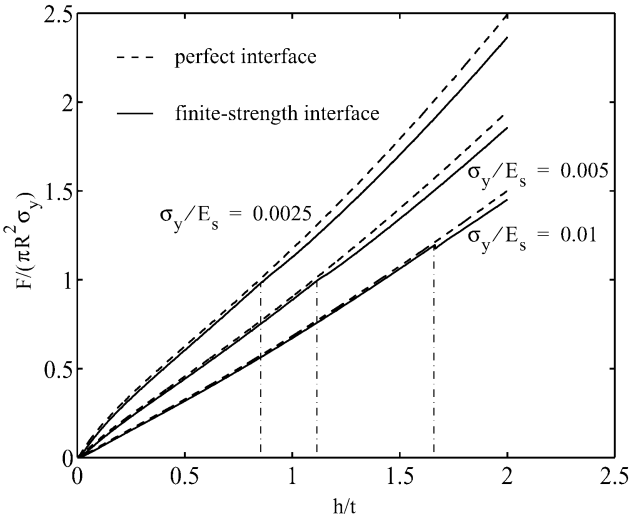

Fig. 11. Normalized load vs. indentation depth curves for different values of σ_y/E_s. Dashed lines represent cases with perfect interface and solid lines represent cases with a finite-strength interface with $\tau_{max}/\sigma_y = 0.6$. The dash-dotted lines identify the initiation values $h = h_c$, (cf. Fig. 6a).

3.6. Load vs. depth of indentation

One of the most common outputs of indentation experiments is the indentation force vs. indentation depth curve (load–displacement curve). Fig. 11 shows the predictions for some of the cases considered here with an interface strength of $\tau_{max}/\sigma_y = 0.6$, in comparison with the corresponding ones for the perfect interface. Prior to initiation of delamination, the results differ very slightly from those with a perfectly bonded

coating, which is just due to the finite stiffness of the cohesive surface. After initiation of the shear delamination, $h > h_c$, the system is noticeably more compliant, yielding an indentation force that is reduced by between 5 and 10% compared to the same case with the perfect interface.

For the smaller yield strengths, the effect of delamination in the $F-h$ curve evolves gradually, but a distinct kink at $h = h_c$ is observed in Fig. 11 for $\sigma_y/E_s = 0.01$. Similar kinks have been observed experimentally by Hainsworth et al. [8] and Li and Bhuchan [9], but they have been associated with through-thickness ring or radial cracks. The kink found here is a result of the high energy release rate at the moment of crack initiation, that gives rise to almost instantaneous growth of the delaminated zone (see Fig. 9a). Since the amount of stored elastic energy is higher for higher interfacial strength and higher substrate yield stress, the kink will be sharper accordingly.

4. Conclusions

Numerical simulations have been carried out of the indentation process of a coated material by a spherical indenter. The interface between the film and the substrate was modeled by a cohesive surface, with a coupled constitutive law for the normal and the tangential response. Failure of the interface by normal or tangential separation, or a combination, is embedded in the constitutive model and does not require any additional criteria.

A parametric study has been carried out to investigate the influence of interfacial strength and substrate yield strength on delamination. Delamination is found to be driven by the shear stress at the interface associated with the plastic deformation in the substrate, and consequently occurs in a tangential mode. Nevertheless, interfacial normal stresses have a significant effect on delamination, due to the coupling between normal and tangential response. Here we have focused on the coupling whereby the interfacial resistance to tangential delamination is reduced by tensile stresses along the interface.

We find, however, that the results are quite sensitive to variations in this coupling so that quantitative predictions require an accurate description of this interface coupling. This pertains, for instance, to the value of the interfacial shear strength above which delamination never occurs. In the absence of any coupling between normal and tangential response, this limiting strength is simply $\tau_{\max} = \sigma_y/\sqrt{3}$, but it is significantly higher due to the coupling. This indicates that especially this coupling in the adopted interface model Eqs. (11) and (12) needs closer examination and comparison with dedicated experiments.

In all cases analyzed, delamination initiates at a radial location that is more than twice the contact radius, and propagates in two directions; towards and away from the indenter, thus generating a ring-shaped delaminated zone. The front which travels towards the indenter gets arrested after a short distance because of the compressive normal stress in that region. After a high initial speed of propagation, the other top settles at a steady propagation at a constant velocity. The initial propagation speed is governed by the high elastic energy stored in the system prior to delamination, while the steady-state speed is controlled by the indentation process itself.

It bears emphasis at this point to recall that the coating is assumed to be elastic and strong. Deviations from this, such as plasticity of the coating or cracking, may affect our findings both for the initiation and the propagation of delamination. As mentioned in Section 1, cracking is a potential mechanism for hard coatings and will change the picture dramatically; this requires a totally different analysis. However, plastic deformation in the hard coatings under consideration will be limited to plastic zones immediately under the indenter, which are often smaller than that in the substrate. In such cases, the precise instant of delamination and the rate of propagation are expected to differ somewhat quantitatively, but to leave the phenomenology essentially unchanged.

For simplicity, the present calculations have assumed perfect but rate-dependent plasticity for the substrate. Rate dependency was never significantly affecting the results here because the time scale for the indentation process was always much larger. Strain hardening of the substrate will, obviously, change the quantitative results, especially for the indentation force vs. depth response. However, we do not expect a qualitatively significant effect on delamination, since the leading front of the delaminated zone seems to propagate with the front of the plastic zone in which hardening has not yet taken place.

Again for simplicity, this study has not accounted for the presence of residual stress in the coating, due for example to thermal mismatch relative to the substrate. This as well as the influence of wavy interfaces will be examined in a forthcoming paper.

References

[1] T.F. Page, S.V. Hainsworth, Surf. Coat. Technol. 61 (1993) 201.
[2] M.V. Swain, J. Menčik, Thin Solid Films 253 (1994) 204.
[3] A. Bagchi, A.G. Evans, Interface Sci. 3 (1996) 169.
[4] B.D. Marshall, A.G. Evans, J. Appl. Phys. 56 (1984) 2632.
[5] M.D. Kriese, W.W. Gerberich, J. Mater. Res. 14 (1999) 3019.
[6] M.D. Drory, J.W. Hutchinson, Proc. R. Soc. London A 452 (1996) 2319.
[7] J.S. Wang, Y. Sugimora, A.G. Evans, W.K. Tredway, Thin Solid Films 325 (1998) 163.

[8] S.V. Hainsworth, M.R. McGurk, T.F. Page, Surf. Coat. Technol. 102 (1997) 97.
[9] X. Li, B. Bhushan, Thin Solid Films 315 (1997) 214.
[10] R. Becker, A. Needleman, O. Richmond, V. Tvergaard, J. Mech. Phys. Solids 36 (1988) 317.
[11] D. Peirce, C.F. Shih, A. Needleman, Comput. Struct. 18 (1984) 875.
[12] X.-P. Xu, A. Needleman, Model. Simul. Mater. Sci. Eng. 1 (1993) 111.
[13] J.H. Rose, J. Ferrante, Phys. Rev. Lett. 47 (1981) 675.
[14] X.-P. Xu, A. Needleman, J. Mech. Phys. Solids 42 (1994) 1397.
[15] M.R. Begley, A.G. Evans, J.W. Hutchinson, Int. J. Solids Struct. 36 (1999) 2773.
[16] S. Sen, B. Aksakal, A. Ozel, Int. J. Mech. Sci. 40 (1998) 1281.
[17] R. Narasimhan, S.K. Biswas, Int. J. Mech. Sci. 40 (1997) 357.